Nucleosome Core Particles Lacking H2B or H3 Tails are Altered Structurally and have Differential Base Excision Repair Fingerprints

*Paul J. Caffrey and Sarah Delaney**

Department of Chemistry, Brown University, Providence, RI 02912

ABSTRACT

A recently discovered post-translational modification of histone proteins is the irreversible proteolytic clipping of the histone N-terminal tail domains. This modification is involved in regulation of various biological process, including the DNA damage response. In this work, we use chemical footprinting to characterize the structural alterations to nucleosome core particles (NCPs) that result from lack of the histone H2B or H3 tails. We also examine the influence of these histone tails on excision of the mutagenic lesion 1,N^6-ethenoadenine (εA) by the repair enzyme alkyladenine DNA glycosylase (AAG). We found that absence of the H2B or H3 tail results in altered DNA periodicity relative to native NCPs. We correlated these structural alterations to εA excision by utilizing a global analysis of 21 εA sites in NCPs and unincorporated duplex DNA. In comparison to native NCPs, there is enhanced excision of εA in tailless H2B NCPs in regions which undergo DNA unwrapping. This enhanced excision is not observed for tailless H3 NCPs, rather, excision is inhibited in more static areas of the NCP not prone to unwrapping. Our results support *in vivo* observations of alkylation damage profiles and the potential role of tail clipping as a mechanism to overcome physical obstructions caused by packaging in NCPs, but also reveal potential inhibition of repair by tail clipping in some locations. Taken together these results further our understanding of how base excision repair can be facilitated or diminished by histone tail removal and contributes to understanding the underlying mechanism that lead to mutational hotspots.

INTRODUCTION

In most eukaryotic organisms, DNA is organized into chromatin. The base unit of packaging in chromatin is the nucleosome core particle (NCP). The NCP is comprised of 145-147 base pairs of DNA wrapped approximately 1.7 times around a histone protein core.[1] The histone core is formed by two copies of each of the proteins H2A, H2B, H3, and H4.[2] Each histone contains a highly structured globular core and an N-terminal disordered tail.[1] There is also a 2-fold rotational axis of pseudosymmetry in the NCP known as the dyad axis. Notably, an NCP is not a static structure but rather a dynamic one where DNA is transiently exposed through unwrapping at the entry/exit points,[3, 4] histone variants can be exchanged for the canonical versions,[5] and histones undergo posttranslational modifications (PTMs).[6, 7] Besides reversible PTMs such as methylation, phosphorylation, and acetylation, proteolytic clipping of the histone tails has been identified as an irreversible modification.[8, 9]

Clipping of the histone tails, particularly H2B and H3, alters the NCP structure and DNA accessibility. It has been shown that the absence of the H3 tail promotes DNA unwrapping and H2A/H2B dimer eviction.[10, 11] Absence of the H2B tail has also been demonstrated to promote DNA unwrapping,[10] putatively via elimination of interactions between the H2B and H3 tails that inhibit unwrapping.[12] Trypsin catalyzed removal of histone tails enhances binding of the GAL4 transcription factor and DNA digestion by restriction enzymes,[13] demonstrating an increase in physical accessibility of DNA in the absence of histone tails. Furthermore, tail removal has been shown to alter the translational positioning of DNA, even when removal was conducted after NCP assembly.[13, 14]

By altering chromatin structure and DNA accessibility, histone tails can play key roles in regulating biological processes. One result of tail clipping is the erasure of PTMs. Moreover, histone clipping itself serves to activate gene expression in yeast,[15] promote cell differentiation,[16]

increase the rate of transcriptional elongation by RNA polymerase,[17] alleviate pausing at promoter regions,[18] and serves as an epigenetic marker.[19] H3 clipping has also been shown to occur under DNA damaging conditions, implicating histone clipping in the DNA damage response.[20]

Single- and double-strand breaks, inter- and intra-strand crosslinks, abasic sites, and modification of the bases are all potential consequences of DNA damaging agents.[21] These various forms of damage are repaired by different pathways. Modified bases, referred to here as lesions, are repaired by the base excision repair (BER) pathway. One mutagenic lesion repaired by the BER pathway is 1,N^6-ethenoadenine (εA, Figure 1).[22, 23] εA is generated both as a byproduct of endogenous lipid peroxidation and exogenous exposure to vinyl chloride.[24, 25] εA levels are elevated in tissues from individuals with chronic inflammatory diseases associated with carcinogenesis as well as cancerous tissues.[26]

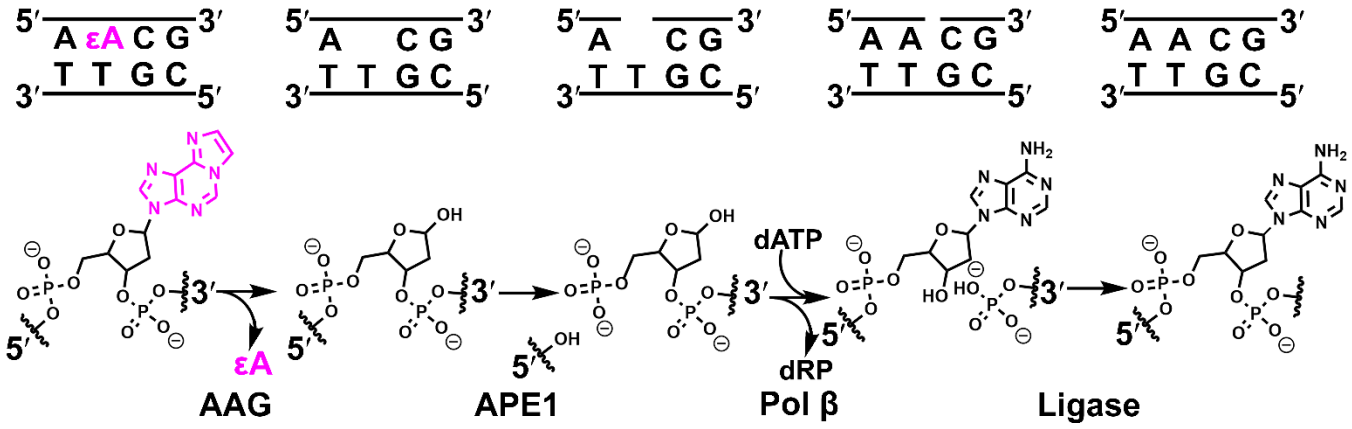

Figure 1. Base excision repair of 1,N^6-ethenoadenine (εA). The εA lesion is shown in pink along with the four steps of the repair catalyzed by AAG, APE1, pol β, and DNA ligase, respectively.

The BER pathway is comprised of several enzymes that catalyze the excision of a lesion and subsequent insertion of an unmodified nucleotide. Alkyladenine glycosylase (AAG) is responsible for excision of alkylated bases, including εA.[27] Excision of εA by AAG results in an apurinic/apyrimidinic (AP) site. This AP site is then incised by AP endonuclease 1 (APE1),

creating a nick with 3'-OH and 5'-deoxyribose phosphate (5'-dRP) termini. Polymerase β (pol β) removes the 5'-dRP and incorporates the correct nucleotide at the 3'-OH. Finally, a DNA ligase completes the repair by sealing the nick in the backbone.[21]

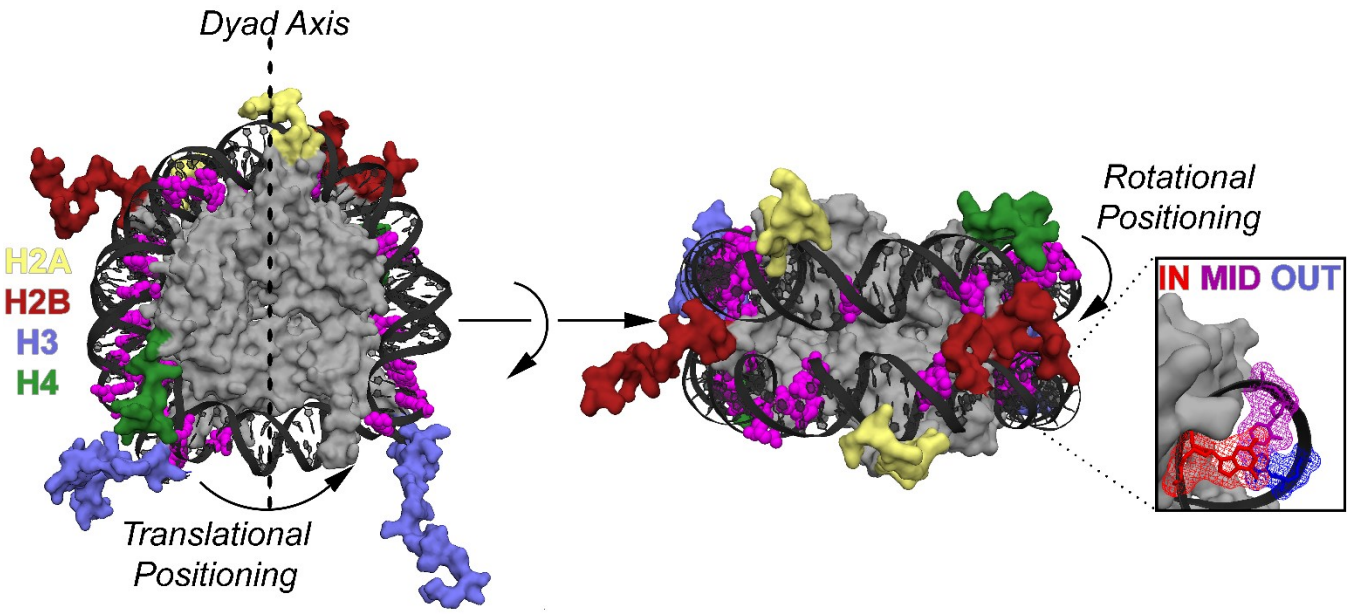

Figure 2. Global distribution of εA lesions in the NCP. The image was created by merging the crystal structure of a 601 NCP lacking histone tails (PDB: 3lz0) with one including tails but with a different DNA sequence (PDB: 1kx5). The location of εA lesions are highlighted in pink. The globular domains of the histones are in gray. The N-terminal tails of each histone are highlighted: H2A (yellow), H2B (red), H3 (blue) and H4 (green). On the left is a top-down view of the NCP with the dyad axis indicated with a dashed line. On the right is a side view after rotating the NCP 90°. Rotational position of bases is shown with examples of IN, MID, and OUT bases provided.

When considering the activity of BER enzymes in an NCP, unlike unpackaged duplex DNA, the geometric positioning of the lesion is important. The dyad axis acts as a reference point in defining the translational position of a lesion (Figure 2). Besides translational positioning, a lesion can be defined by its rotational orientation which can be described as outwards towards solution (OUT), inwards towards the histone core (IN), or somewhere in between (MID). Further

microenvironments are created by the DNA superhelices, histone tails, and areas of transient unwrapping of DNA from the histone core.

In this work, we use chemical footprinting techniques to show that NCPs lacking either the H2B or H3 tail have structures distinct from NCPs with intact tails. We also demonstrate that these structural differences manifest in differential excision of εA by AAG. Excision is enhanced in the entry/exit regions of NCPs lacking H2B tails, but inhibition is seen in less dynamic areas of the NCPs lacking H3 tails. Taken together, these results implicate tail removal as a potential modulator of BER initiation in chromatin.

MATERIALS AND METHODS

Oligonucleotide Synthesis and Purification

All oligonucleotides used in this study were synthesized on a MerMade 4 DNA synthesizer (BioAutomation). We used the 145 bp Widom 601 nucleosome positioning sequence (Scheme S1) as the unincorporated duplex control and to assemble NCPs. Synthesis of the 145 mer oligonucleotide containing εA was conducted on 1,400 Å controlled pore glass beads (BioAutomation) using phosphoramidites with ultramild protecting groups (Glen Research). Deprotection was performed according to the manufacturer's specifications. εA substitution for A throughout the "I" strand was conducted utilizing a Poisson distribution, as described in recent reports.[28-30] The molar ratio determined by the Poisson distribution ($\lambda = 0.355$) was used to determine the correct mixture of A and εA phosphoramidites. This synthetic strategy yields a DNA population containing either 0 or 1 εA lesion per 145 mer oligonucleotide while minimizing strands containing two or more lesions to 5% of the population. Numbering starts with the first base of the 5′-end of the "I" strand. The final trityl group was removed on the synthesizer, and the DNA

cleaved from the solid support by incubation in NH_4OH at room temperature for 2 h. The DNA was then purified via the crush and soak method utilizing 8% denaturing polyacrylamide gel electrophoresis (PAGE).

A ligation strategy was utilized to prepare the complementary 145 mer (Scheme S2). The component oligonucleotides for ligation were synthesized using standard phosphoramidite protecting groups with the final trityl group retained. Reverse-phase HPLC purification at 90 °C was used to purify the oligonucleotides (Agilent PLRP-S column, 250 mm × 4.6 mm; A = 100 mM triethylammonium acetate [TEAA] in 5% aqueous MeCN, B = 100 mM TEAA in MeCN; 5:95 to 35:65 A:B over 30 min, 35:65 to 5:95 A:B over 5 min at 1 mL/min). Removal of the trityl group was accomplished by incubation in 20% v/v aqueous glacial acetic acid for 1 h at room temperature. Subsequently, a second HPLC purification at 90 °C was performed (Agilent PLRP-S column, 250 mm × 4.6 mm; A = 100 mM triethylammonium acetate [TEAA] in 5% aqueous MeCN, B = 100 mM TEAA in MeCN; 0:100 to 15:85 A:B over 35 min, 15:85 to 35:65 A:B over 5 min at 1 mL/min). Electrospray ionization mass spectrometry was used to verify the identity of the component oligonucleotides. Five nmol of each component oligonucleotide J2 and J3 were 5′-phosphorylated using 2 mM ATP and T4 kinase (New England Biolabs). These phosphorylated components were then combined in equal molar amounts with component J1 and 10% excess of two scaffolding oligonucleotides, JS12 and JS23, and annealed by heating to 95 °C for 5 min and cooling at 1°C per min in 50 mM NaCl and 20 mM Tris (pH 8.0). These annealed oligonucleotides were then ligated at room temperature overnight using 4,800 units T4 DNA ligase in buffer (50 mM Tris-HCl, 10 mM NaCl, 10 mM $MgCl_2$, 10 mM DTT, 1 mM ATP, pH: 7.5). The product of the ligation reaction was then purified using 8% denaturing PAGE.

For normalization of AAG glycosylase excision data (*vide infra*), a 23 mer and a 92 mer were designed as internal standards such that they would not co-migrate with any εA cleavage product. They were synthesized as described above and purified by 12% and 8% denaturing PAGE, respectively.

Reconstitution of Global εA Nucleosome Core Particles

Recombinant *Xenopus laevis* histones were expressed and purified individually before assembly into octamers.[31, 32] The globular *X. laevis* H2B protein (residues 24-122) and H3 protein (residues 38-135) were purchased from The Histone Source (Colorado State University). NCPs were reconstituted as described previously[31] via salt gradient dialysis of the radiolabeled εA-containing duplex population and histone octamer. Briefly, a molar excess of histone octamer was added to εA containing 145 bp duplex with a ^{32}P radiolabel attached at the 5'-end (10.05 pmol octamer to 10.00 pmol DNA for gH3 NCP, 10.10:10.00 pmol for native NCP, and 10.15:10.00 pmol for gH2B NCP) in buffer (10 mM Tris-HCl [pH 7.5], 1 mM EDTA, 1 mM dithiothreitol [DTT], 2 M NaCl, 500 μg/mL BSA) in a Slide-a-Lyzer dialysis device (0.1 mL capacity, 3.5 kDa MWCO; Thermo Fisher Scientific). The dialysis device started in a buffer of 10 mM Tris-HCl (pH 7.5), 1 mM EDTA, 1mM dithiothreitol (DTT), 2 M NaCl at 4 °C before transfer to buffers containing decreasing concentrations of NaCl (1.2 M, 1.0 M, 0.6 M, 0 M) at hourly intervals. The final dialysis in 0 M buffer was conducted for 3 h and then the NCPs were filtered with a 0.45 μm cellulose acetate centrifuge tube filter (Corning Costar) to remove insoluble particles. NCP formation and relative purity were analyzed using a 7% native PAGE (60:1 acrylamide: bisacrylamide; 0.25X TBE) run for 3 h at 160 V in 4 °C (Figure S1). Only NCPs containing < 5% duplex were used in these studies.

Hydroxyl Radical Footprinting

To determine the rotational orientation of bases in the NCPs we utilized hydroxyl radical footprinting. To ensure single hit conditions we used a modified version of the method of Tullius.[33, 34] Briefly, 7.5 μL of each 1 mM Fe(II)-EDTA, 10 mM sodium ascorbate, and 0.12% w/v aqueous hydrogen peroxide were combined with 5 pmol NCPs in a total of 52.5 μL buffer (10 mM Tris-HCl [pH 7.5], 1 mM EDTA). This mixture was incubated in the dark at room temperature for 10 min and then quenched with 16 μL 1 mM EDTA in 25% v/v glycerol and immediately loaded onto a 7% native PAGE (60:1 acrylamide: bisacrylamide; 0.25x TBE) which was run for 3 h at 155 V at 4 °C. The gel bands containing NCPs were excised and eluted into buffer (0.3 M NaOAc, 1 mM Tris-HCl [pH 8.0], 1 mM EDTA) for 18-24 h at 37°C with gentle shaking (60 rpm). The eluent was then concentrated using a centrifugal concentrator (Sartorius Viaspin Turbo 15, 5 kDa MWCO) and filtered using a 0.22 μm cellulose acetate syringe filter. The samples were extracted with equal volume addition of 25:24:1 phenol:chloroform:isoamyl alcohol (PCI) and the aqueous layer was concentrated by SpeedVac evaporation. Following the addition of 40 μL co-precipitation agent (0.5 mg/mL tRNA in 300 mM NaOAc [pH 8.0], 1 mM EDTA), samples were desalted with ethanol precipitation. Samples were resuspended in a 1:1 mixture of formamide and water for denaturing PAGE. Cleavage fragments were resolved by 8% denaturing PAGE (Figure S2) and quantitated using SAFA[35] gel analysis software. The highest band intensity within a helical turn was used to normalize the data and correct for loss of smaller DNA fragments during workup. To accomplish this normalization, the band intensities were plotted against base position to identify the maxima and minima corresponding to OUT and IN locations, respectively. The five bases flanking to each side of a maximum were divided by the maximum band intensity to normalize the values within each helical turn. A three point smooth was then applied and MATLAB used for a

single term Fourier fitting of bases 20-80 for each NCP to the following general equation: $f(x) = a0 + a1 * \cos(x * w) + b1 * \sin(x * w)$ where $a0,\ a1, \text{and}\ b1$ are the Fourier coefficients and w is the fundamental frequency, w. Only fits with an R squared value of ≥ 0.7 were used for period determination. The period was determined using the following equation: $T = 2\pi/w$.

Enzymatic Reactions

Human AAG was purchased from New England Biolabs, and the total enzyme concentration determined by Bradford assay using γ-globulin standards (Bio-Rad Laboratories). AAG excision was assessed by mixing 1 pmol substrate (either duplex DNA or native, gH2B, or gH3 NCPs) with 40 pmol AAG in a total volume of 20 µL of the reaction buffer (20 mM Tris, 50 mM NaCl, 150 mM KCl, 1 mM DTT, 100 µg/mL BSA) and incubated for 1 h at 37 °C along with a negative control sample (no enzyme). After 1 h, samples were quenched with 20 µL of 1M NaOH which had been spiked with the radiolabeled internal standards and heated to at 90 °C for 3 min. PCI extraction separated the DNA from protein and the aqueous layer was supplemented with 40 µL co-precipitation agent (0.5 mg/mL tRNA in 300 mM NaOAc [pH 8.0], 1 mM EDTA) and 600 µL of ethanol before being placed on dry ice for 30 min. The ethanol was then separated from the DNA via centrifugation, removed with a pipette, and all samples were resuspended in 50% v/v formamide:water, split in half, and loaded onto an 0.6 mm, 8% PAGE gel (Figure S3). One half of the samples were loaded to resolve bands 19-64, run 2 h at 80 W. The other half of the samples were loaded to resolve of bands 89-123, run 4 h at 80 W.

After phosphorimaging of the gels, SAFA software was used to quantitate band intensity. The internal standards were used for band normalization, sites 19-64 with the 23 mer standard and sites 89-123 with the 92 mer standard. The no enzyme control was used to subtract background from enzyme-treated samples. For each site, the ratio of corrected band intensity in the NCPs to

the duplex was used to determine the NCP/Duplex (NCP/DUP) ratio for AAG activity. An NCP/DUP value of 1 indicates excision that is comparable to duplex, while a value below one indicates lower excision in NCPs relative to duplex. The standard error (SE) of NCP/DUP was calculated using $SE = \sigma/\sqrt{(n)}$, where σ is the standard deviation of the population and n is the sample size. For all NCPs n=3. A two-tailed Welch's *t* test (α=0.05) was performed to obtain the p value at each εA site for NCP/DUP for each tailless NCP in comparison to native NCP/DUP. All statistical analyses were conducted using R. We considered $p < 0.05$ to be significant.

RESULTS

Preparation of NCPs Containing Globally Substituted εA Lesions

To examine the effects of H2B and H3 tail deletion on the excision activity of AAG, NCPs were assembled using the Widom 601 DNA sequence and recombinant histones.[36] The NCPs had three combinations of histones: all full length histones (native NCP); native H2A, H3, H4 and globular (tailless) H2B domain (gH2B NCP); or native H2A, H2B, H4 and globular (tailless) H3 domain (gH3 NCP). Using the 601 DNA creates a homogenous population of NCPs as a substrate for biochemical studies, since it is a strong positioning sequence that reproducibly binds the histone octamer in a single translational and rotational position.[36] Furthermore, crystal structures of 601 NCPs, albeit without histone tails, are available for reference.[36]

εA lesions were incorporated throughout the "I" strand of the Widom 601 sequence to create a population of DNA containing εA:T base pairs, utilizing methods we reported previously.[28-30, 37] (The "I" strand designation is based on nomenclature used in the reported crystal structure of the 601 NCP.[36]) Briefly, a Poisson distribution was used to determine the molar ratio of A to εA phosphoramidite building blocks used during chemical synthesis such that 95% of the

synthesized DNA contain no more than a single εA. Overall, we examined excision of εA from 21 sites to define the repair fingerprint of AAG in native, gH2B, and gH3 NCPs.

HRF Reveals Structural Differences in Native NCPs Compared to gH2B and gH3 NCPs

We utilized hydroxyl radical footprinting (HRF) to establish the rotational orientation of each base and determine the periodicity of DNA in the NCPs.[34] When DNA is packaged in an NCP, an oscillatory pattern of high and low reactivity towards hydroxyl radicals is observed. This pattern emerges from the preferential abstraction of C5' hydrogens of the sugar-phosphate backbone facing away from the histone core,[38] while C5' hydrogens facing towards the histone core are shielded and protected from hydroxyl radicals.

Quantitation of the HRF for each NCP confirms varying levels of solution accessibility throughout the DNA and establishes the rotational orientation of each base (Figure 3, Figure S2, Table S1). OUT sites, defined here as a maximum in the HRF profile, demonstrate the highest HRF reactivity. IN sites, defined here as a minimum in the HRF profile, exhibit the lowest HRF reactivity. MID sites, defined here as a being between a minimum and maximum in the HRF profile, demonstrate intermediate HRF reactivity. The distribution of rotational orientation of εA lesions varied and we examined AAG activity at 5 OUT, 5 MID, and 11 IN lesion sites (Table 1).

Table 1. Translational position, rotational orientation, and AAG excision activity for native, gH2B, and gH3 NCPs. Statistical significance ($p < 0.05$) of εA excision relative to native NCP is indicated by *.

Translational Base Position	Rotational Orientation	AAG Excision Activity (NCP/DUP)		
		Native NCP	gH2B NCP	gH3 NCP
19	IN	0.21	0.21	0.02*
28	IN	0.03	0.08*	0.03
29	IN	0.07	0.07	0.02
38	IN	0.06	0.02	0.02
40	MID	0.19	0.01	0.03
42	OUT	1.02	0.91	0.63
48	IN	0.00	0.01	0.02
51	MID	0.47	0.55	0.12*
58	IN	0.00	0.04*	0.02
59	IN	0.00	0.03	0.04
60	IN	0.00	0.02	0.08
64	OUT	0.84	1.04*	0.67
89	IN	0.02	0.05	0.00
90	IN	0.00	0.01	0.00
96	OUT	1.02	0.78	0.33*
97	OUT	0.37	0.17	0.13
102	MID	0.04	0.27	0.12
105	MID	1.11	1.00	0.62
112	MID	0.02	0.44*	0.25
119	IN	0.13	0.61*	0.40
123	OUT	0.77	0.81	0.95

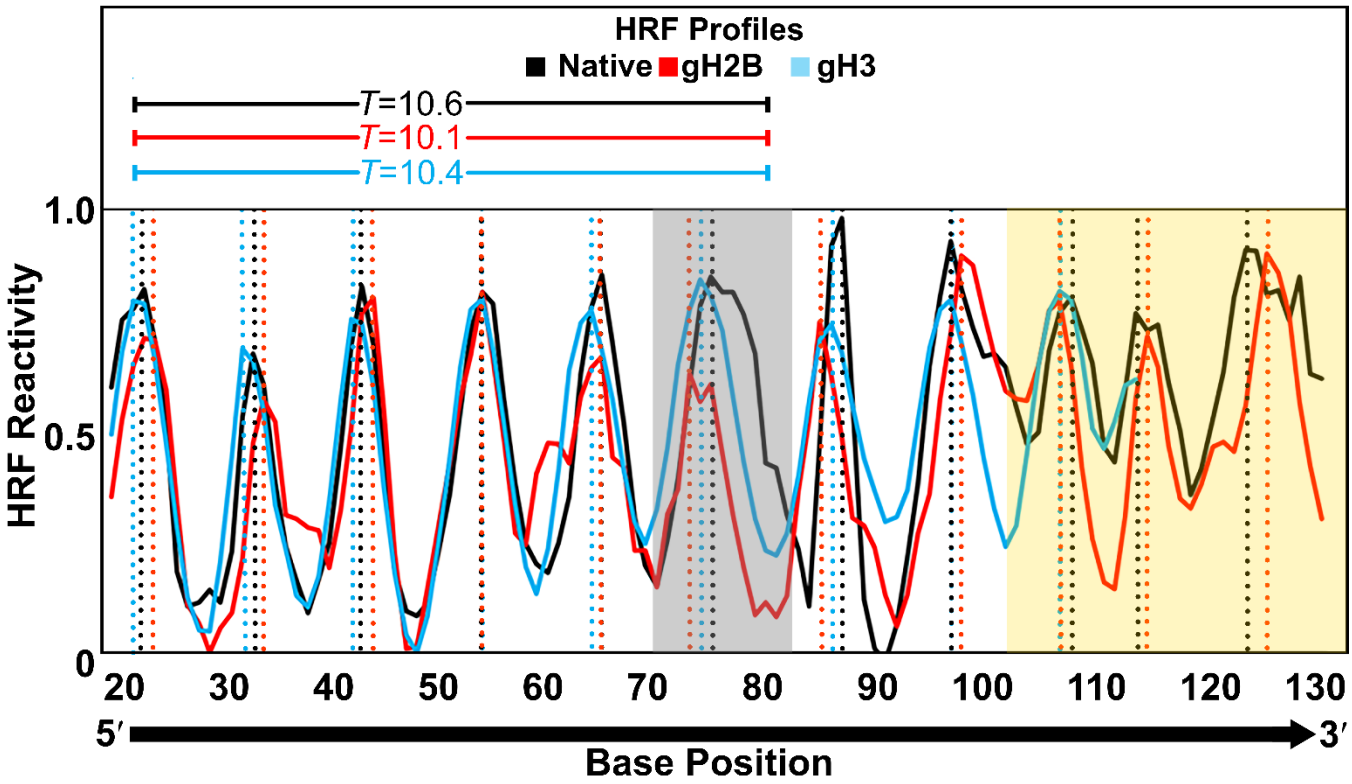

Figure 3. HRF profiles for native (black), gH2B (red), and gH3 (blue) NCPs with dashed vertical lines indicating maximum locations. The yellow highlighting indicates DNA near the entry/exit region in the NCP. Gray highlighting indicates the dyad region. The average periodicity (T) from bases 20-80 for each NCP is indicated.

Comparison of the HRF profiles of the native (black), gH2B (red), and gH3 (blue) NCPs reveals structural differences (Figure 3). The profiles of all three NCPs exhibit the expected oscillatory pattern. However, there are differences in locations of the maxima and minima for many helical turns. For example, the native NCP has a maximum at position 33 (vertical black dashed line) while gH2B (red dashed) is at 32 and gH3 (blue dashed) at 34. Differences in locations of maxima and minima can be seen throughout the NCP, with the only shared maxima for all three NCPs at 54. Other shared maxima can be seen for gH2B and gH3 NCPs at 107; gH2B and native NCPs at 65; and gH3 and native NCPs at 97. Differences in the location of maxima and minima indicate differential stretching and compaction of the DNA in these NCPs.

Alterations to the shape of the HRF profiles are observed near the dyad axis (Figure 3, gray shaded region). The native NCP has a broad maximum while the gH2B and gH3 NCPs display narrower peaks. The broader maximum indicates an area facing OUT that is underwound in the native NCP relative to the gH2B and gH3 NCPs. Changes continue towards the 3'-end for all NCPs. A Fourier fit of bases 20-80 reveals that the average periodicity, the number of base pairs per helical turn, differs between the three NCPs: 10.6 bp/turn for native NCP, 10.1 bp/turn for gH2B NCP, and 10.4 bp/turn for the gH3 NCP. Poor fits for bases 90-130 and lack of data for gH2B NCPs beyond base 115 prevented a periodicity analysis for the 3'-end.

Excision of εA from Native NCPs Correlates with Rotational Orientation

AAG is known to remove εA from duplex DNA not packaged into NCPs (unincorporated duplex).[23, 39, 40] To determine the effects of incorporation into an NCP on εA excision we compared excision from each NCP as a ratio relative to unincorporated duplex (NCP/DUP). A ratio of 1 indicates that excision from NCPs is comparable to unincorporated duplex, while a ratio less than 1 indicates inhibition of excision from NCPs.

The repair fingerprint of native NCPs demonstrates a strong correlation between rotational orientation and AAG excision (Figure 4, black bars; Table 1). Low AAG excision (NCP/DUP <0.2) is observed for IN sites. In contrast, high excision (NCP/DUP >0.6) is observed for most OUT sites with the notable exception being site 97 (Figure 5, black bars), with NCP/DUP of <0.4. MID sites demonstrate much more variability, with most NCP/DUP ranging between 0.1-0.6, except site 105 which reaches 1. This correlation between rotational orientation and excision is in agreement with previous reports.[28, 37]

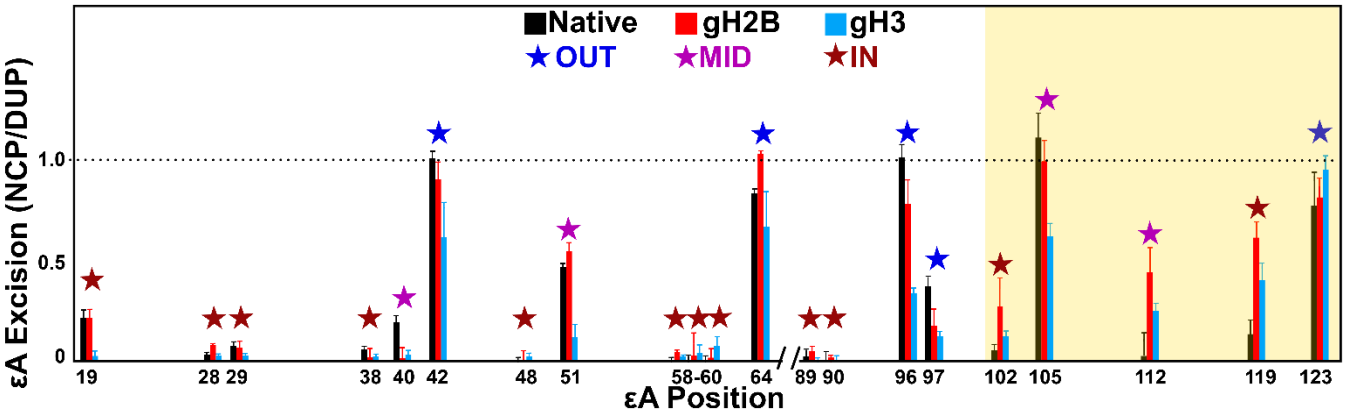

Figure 4. AAG excision activity for native (black), gH2B (red), and gH3 (blue) NCPs. Stars indicate rotational orientation: OUT (blue), MID (purple) and IN (dark red) as determined by HRF. The yellow highlighting indicates the region outside of the central DNA in the NCP.

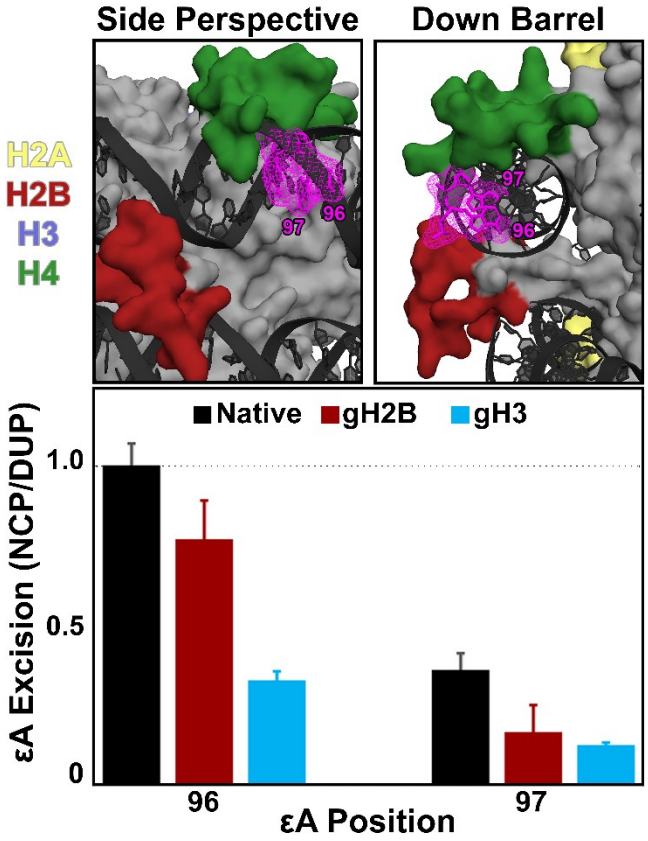

Figure 5. Location of εA sites 96 and 97 in the NCP compared to their excision activity. (Top) The side perspective (left) and down barrel perspective (right) of εA sites 96 and 97 are highlighted in the NCP. (Bottom) The AAG excision activity are shown for each NCP: native (black), gH2B (red), and gH3 (blue).

Excision of εA from gH2B

For the majority of εA lesions, excision is comparable or enhanced in gH2B compared to native NCPs (Figure 4, red bars; Table 1). Enhancement is particularly notable in the DNA entry/exit region (Figure 4, yellow shaded region). Like the native NCPs, there is a general correlation between rotational position and εA excision in the central region of the NCP (bases 19-97), with OUT sites exhibiting generally higher NCP/DUP values than IN or MID sites. There is a small, but significant enhancement of εA excision at OUT site 64 and IN sites 28 and 58 in the gH2B NCP. However, in contrast to native NCPs, the IN and MID sites located towards the 3'-end of the sequence (112 and 119) show 5-22 fold enhancement in excision (Figure 6, red bars). Sites 42, 48, and 51 are on the same DNA superhelix but on the opposite side of the H2B tail but do not exhibit similar enhancement of excision. There are no sites that show significant inhibition in the gH2B NCP compared to native NCP.

Excision of εA from gH3 NCPs

Unlike the gH2B NCPs, which show a few sites of enhanced excision compared to native NCPs, gH3 NCPs show no significant enhancement at any site (Figure 4, blue bars; Table 1). In contrast, the AAG repair profile for gH3 NCPs displays inhibitory effects in the central part of the NCP compared to native NCPs (Figure 4, blue bars). Excision at IN (19), MID (51), and OUT (96; Figure 5) sites is inhibited and varies from 3 to 10-fold.

DISCUSSION

In this work, we compare the global repair profiles of AAG on εA lesions distributed throughout native NCPs or those lacking H2B or H3 tails. As observed previously, εA removal by AAG is highly correlated with rotational orientation in the central region of the DNA in native NCPs.[28, 37] We also reported a similar trend for the glycosylases 8-oxo-7,8-dihydroguanine

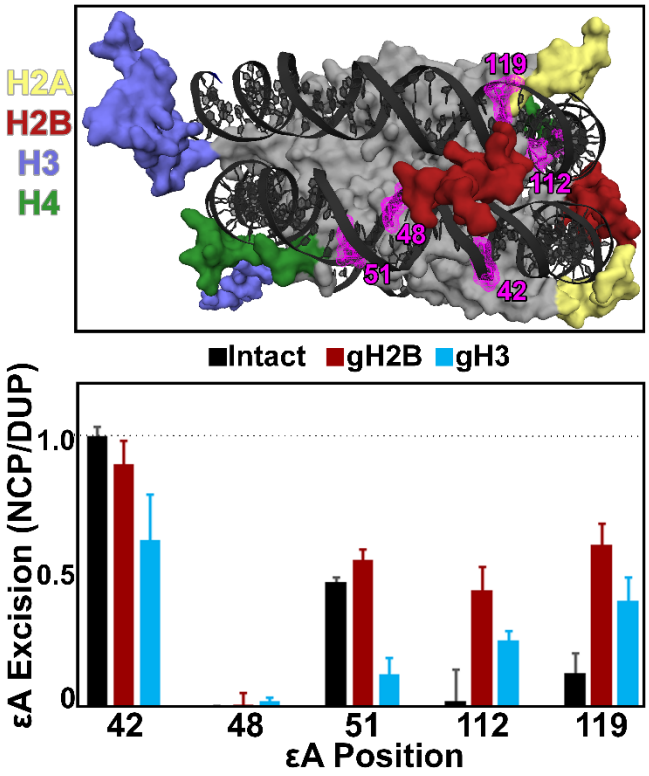

Figure 6. Location and excision of selected εA sites. (Top) The location of selected εA sites and histone tails are highlighted. (Bottom) The AAG excision activity for each NCP: native (black), gH2B (red), and gH3 (blue).

glycosylases (OGG1),[30, 41] uracil DNA glycosylase (UDG),[29, 41] and thymine DNA glycosylase (TDG).[42] A correlation between rotational orientation of a lesion and glycosylase activity has also been reported by other groups.[43-46]

There have been limited studies of the effects of histone tails on BER. Digestion of histone tails by trypsin had a minimal effect on UDG activity.[47, 48] APE1 incision activity was also not affected.[48] When a portion of the H2B tail, known as the histone H2B repression (HBR) domain, is deleted, enhanced UDG and pol β activity are observed in the entry/exit regions.[49] This enhanced activity was attributed to DNA unwrapping in the absence of the HBR domain. Finally, DNA ligase 1 activity was reported to be enhanced in the dyad region following trypsin digestion of the histone tails.[50]

Examination of BER of alkylation damage in yeast with H2A or H3 tail deletions demonstrated the roles of the tails in the regulation of glycosylase expression, DNA damage signaling, and post replicative repair.[51] The removal of tails resulted in diminished cell survival upon treatment with alkylating agents, even when the glycosylase responsible for excision of alkylation damage in yeast, Mag1 (the homolog of AAG), was overexpressed.

When interpreting the repair fingerprint of AAG activity on native, gH2B, and gH3 NCPs we considered that removal of the H2B or H3 could eliminate a steric block and lead to increased accessibility of nearby lesions. Sites 42, 48, 51, 102, 112, and 119 are located near the H2B tail (Figure 6) and distributed both in the central region of the DNA as well as the DNA entry/exit region. No significant enhancement in excision of lesions in the central region of the DNA was observed in the absence of the H2B or H3 tails. In fact, gH3 NCPs demonstrate inhibited εA excision relative to native NCPs at site 51. While the lesions near the DNA entry/exit region exhibit enhanced excision by AAG in gH2B NCPs, we do not ascribe this increase to removal of a steric block caused by the tail, but rather altered DNA structure and dynamics as discussed below.

Changes in the DNA periodicity in the absence of histone tails may affect εA excision. The excision at site 51 in the native NCP compared to the gH3 NCP demonstrates this potential effect. Despite being a MID site in both NCPs, there is significant inhibition of εA excision in the gH3 NCP. There are no tails in the crystal structure that interact with directly this position, so it is unlikely to be a steric effect from tail removal. The underwinding of the DNA helix in the gH3 NCP relative to the native NCP within this helical turn may help explain this result. The altered periodicity may be inhibitory to binding or substrate recognition by AAG. This effect of altered periodicity of the DNA in the central part of the NCP may, in part, explain more broadly the inhibitory effects of tail removal in this region.

While the DNA in the central part of the NCP does not unwrap, the DNA located in the entry/exit region of native NCPs is known to unwrap transiently and spontaneously to expose sites that would be otherwise occluded. For the Widom 601 "I" strand it has been shown that the 3'-end preferentially unwraps.[56] We have reported previously that glycosylase activity, including AAG, does not correlate with rotational orientation in certain translational locations prone to unwrapping.[29, 30, 41] Unwrapping has also been reported to be rate-limiting for the activity of endonuclease III-like protein 1 (NTH1) glycosylase [57, 58] and to be exploited by Nap1 during H2A/H2B dimer eviction.[59]

We find that lesions located near the DNA entry/exit region are better excised in NCPs lacking the H2B but not the H3 tail. Computational studies have predicted enhanced unwrapping when histone tail charges are neutralized, which is particularly pronounced for the H2B and H3 tails.[12, 60] This charge neutralization stabilizes unwrapped states out to 40 base pairs for H2B and 30 base pairs for H3 under salt conditions similar to those used in our study. For comparison, native NCPs demonstrate unwrapping of ~20 base pairs. Crystal structures have revealed that H2B and H3 tail deletion weakens histone interactions with DNA and undermines the stability of the NCP.[10] Similar observations were made by SAXS[61] and FRET[62, 63] which demonstrated enhanced dynamics and nucleosomal instability upon tail removal. Our results are consistent with the notion that removal of the H2B tail promotes greater DNA unwrapping from the histone proteins and this unwrapping allows for excision of otherwise occluded εA lesions by AAG. However, the removal of the H3 tail does not promote similar enhancement of εA excision, possibly due to a lesser degree of unwrapping than observed upon H2B tail removal.

While structural alterations and enhanced unwrapping of the DNA in the NCP explain the observations above, it is also important to consider interactions between the histone protein

themselves. Interactions between the histone tails may explain some of the inhibition of AAG activity. Histone tails are essential for formation of nucleosomal arrays through extensive intra- and inter-nucleosomal contacts.[52] Even the presence of a bulky lesion in the DNA near the H2B tail has been simulated to change tail conformation.[53] Removal of εA at site 96, near the H2B and H4 tails (Figure 5), is significantly inhibited by H3 tail removal but not H2B tail removal. Surprisingly, the shift of the HRF maximum in this region to position 97, making it more OUT, for the gH3 NCP does not enhance εA excision. The H4 tail, important for inter-nucleosomal interactions,[54] in this region may undergo a conformational change in the absence of the H3 tail that inhibits AAG binding or excision activity. These potential synergistic tail-tail interactions are not unexpected as computational studies have shown that the acetylation of the H4 tail impacts the ability of the H3 tail to interaction with other proteins.[55] Similarly, the maximum shift from position 65 to position 64, making it a more OUT lesion, in the gH3 NCP does not confer enhanced εA excision. In contrast, the gH2B NCPs show a small enhancement of activity while retaining the same maximum at position 65 seen in native NCPs. The enhancement of excision at site 64 in the gH2B without a change in DNA periodicity and absent any steric interactions with the H2B tail indicate other modulating protein-protein interactions. Taken together these results indicate that it is not only DNA-protein contacts that affect εA excision in NCPs, but also protein-protein interactions. Only by taking all these factors cumulatively can the repair fingerprint of AAG in these varied NCPs be understood.

Biological observations of mutational hotspots and accumulation of alkylation damage can also be considered in light the results obtained here. In yeast, it has been reported that alkylation damage accumulates at IN lesions.[64] Such sites were also observed to be mutational hotspots in the analysis of human tumors.[65] These data suggests the need for alternate mechanisms to access

these IN sites for repair, such enhanced unwrapping of DNA from histones. Indeed, H2B[60] and H3[6] acetylation has been shown to enhance DNA unwrapping and acetylation has been observed to occur as part of the DNA damage response.[66] More intriguingly, it has been recently reported that a complex is formed between AAG and RNA polymerase II that may access occluded lesions by utilization of chromatin decondensation.[67] This complex, along with the observation that the H3 tail protease JMJD5 relieves RNA polymerase II pausing[18] and the protease is active under DNA damaging conditions,[20] implicates tail clipping as a mechanism to repair DNA damage during transcription. Together with these findings, our results indicate a potential mechanism to access DNA damage by the BER pathway: utilizing tail clipping to promote DNA accessibility through unwrapping from the histone octamer.

SUPPORTING INFORMATION

The Supporting Information is available free of charge on the ACS Publications website.

DNA sequences and schemes, supplementary figures and tables (including gel images, hydroxyl radical footprinting, and normalized HRF reactivity values).

AUTHOR INFORMATION

Corresponding Author
*Email: sarah_delaney@brown.edu. Phone: +1 401 863 1000.

ORCHID
Sarah Delaney: 0000-0002-8366-3808
Paul J. Caffrey: 0000-0003-4208-8621

Funding
This research was supported by the National Science Foundation (MCB-1817417).

Notes
The authors declare no competing financial interest.

ACKNOWLEDGMENT

This research was supported by the National Science Foundation (MCB-1817417).

ABBREVIATIONS

AAG, alkyladenine glycosylase; BER, base excision repair; DUP, unpackaged duplex DNA; εA, 1,N^6-ethenoadenine; gH2B, globular H2B; gH3, globular H3; HRF, hydroxyl radical footprinting; NCP, nucleosome core particle; PAGE, polyacrylamide gel Electrophoresis; SAFA, semi-automated footprinting analysis

ACCESSION CODES

X. Laevis H2A Uniprot entry Q6AZJ8, *X. Laevis* H2B Uniprot entry P02281; *X. Laevis* H3 Uniprot entry P84233; *X. Laevis* H4 Uniprot entry P62799; *H. Sapien* AAG Uniprot entry P29372

REFERENCES

1. Luger, K., Mäder, A. W., Richmond, R. K., Sargent, D. F., Richmond, T. J. (**1997**) Crystal structure of the nucleosome core particle at 2.8 Å resolution. *Nature 389* (6648), 251-260. DOI: 10.1038/38444
2. Eickbush, T. H. and Moudrianakis, E. N. (**1978**) The histone core complex: an octamer assembled by two sets of protein-protein interactions. *Biochemistry 17* (23), 4955-4964. DOI: 10.1021/bi00616a016
3. Lee, J. Y., Lee, J., Yue, H., Lee, T. H. (**2015**) Dynamics of nucleosome assembly and effects of DNA methylation. *J. Biol. Chem. 290* (7), 4291-303. DOI: 10.1074/jbc.M114.619213
4. Zhou, K., Gaullier, G., Luger, K. (**2019**) Nucleosome structure and dynamics are coming of age. *Nat. Struct. Mol. Biol. 26* (1), 3-13. DOI: 10.1038/s41594-018-0166-x
5. Venkatesh, S. and Workman, J. L. (**2015**) Histone exchange, chromatin structure and the regulation of transcription. *Nat. Rev. Mol. 16* (3), 178-189. DOI: 10.1038/nrm3941
6. Gansen, A., Tóth, K., Schwarz, N., Langowski, J. (**2015**) Opposing roles of H3- and H4-acetylation in the regulation of nucleosome structure - A FRET study. *Nucleic Acids Res. 43(3) 1433-43*. DOI: 10.1093/nar/gku1354
7. Kim, J., Lee, J., Lee, T.-H. (**2015**) Lysine Acetylation Facilitates Spontaneous DNA Dynamics in the Nucleosome. *J. Phys. Chem. B 119* (48), 15001-15005. DOI: 10.1021/acs.jpcb.5b09734
8. Campos, E. I. and Reinberg, D. (**2009**) Histones: Annotating Chromatin. *Annu. Rev. Genet. 43* (1), 559-599. DOI: 10.1146/annurev.genet.032608.103928

9. Azad, G. K., Swagatika, S., Kumawat, M., Kumawat, R., Tomar, R. S. (**2018**) Modifying Chromatin by Histone Tail Clipping. *J. Mol. Biol. 430* (18, Part B), 3051-3067. DOI: 10.1016/j.jmb.2018.07.013
10. Iwasaki, W., Miya, Y., Horikoshi, N., Osakabe, A., Taguchi, H., Tachiwana, H.; Shibata, T., Kagawa, W., Kurumizaka, H. (**2013**) Contribution of histone N-terminal tails to the structure and stability of nucleosomes. *FEBS Open Bio 3*, 363-9. DOI: 10.1016/j.fob.2013.08.007
11. Ferreira, H., Somers, J., Webster, R., Flaus, A., Owen-Hughes, T. (**2007**) Histone Tails and the H3 αN Helix Regulate Nucleosome Mobility and Stability. *Mol. Cell. Biol. 27* (11), 4037-4048. DOI: 10.1128/MCB.02229-06
12. Kenzaki, H. and Takada, S. (**2015**) Partial Unwrapping and Histone Tail Dynamics in Nucleosome Revealed by Coarse-Grained Molecular Simulations. *PLoS Comput. Biol. 11* (8), e1004443-e1004443. DOI: 10.1371/journal.pcbi.1004443
13. Polach, K. J., Lowary, P. T., Widom, J. (**2000**) Effects of core histone tail domains on the equilibrium constants for dynamic DNA site accessibility in nucleosomes. *J. Mol. Biol. 298* (2), 211-223. DOI: 10.1006/jmbi.2000.3644
14. Yang, Z., Zheng, C., Hayes, J. J. (**2007**) The core histone tail domains contribute to sequence-dependent nucleosome positioning. *J. Biol. Chem. 282* (11), 7930-8. DOI: 10.1074/jbc.M610584200
15. Santos-Rosa, H., Kirmizis, A., Nelson, C., Bartke, T., Saksouk, N., Cote, J., Kouzarides, T. (**2009**) Histone H3 tail clipping regulates gene expression. *Nat. Struct. Mol. Biol. 16* (1), 17-22. DOI: 10.1038/nsmb.1534
16. Kim, K., Punj, V., Kim, J.-M., Lee, S., Ulmer, T. S., Lu, W., Rice, J. C., An, W. (**2016**) MMP-9 facilitates selective proteolysis of the histone H3 tail at genes necessary for proficient osteoclastogenesis. *Genes Dev. 30* (2), 208-219. DOI: 10.1101/gad.268714.115
17. Protacio, R. U., Li, G., Lowary, P. T., Widom, J. (**2000**) Effects of histone tail domains on the rate of transcriptional elongation through a nucleosome. *Mol. Cell. Biol. 20* (23), 8866-8878. DOI: 10.1128/mcb.20.23.8866-8878.2000
18. Liu, H., Ramachandran, S., Fong, N., Phang, T., Lee, S., Parsa, P., Liu, X., Harmacek, L., Danhorn, T., Song, T., Oh, S., Zhang, Q., Chen, Z., Zhang, Q., Tu, T.-H., Happoldt, C., O'Conner, B., Janknecht, R., Li, C.-Y., Marrack, P., Kappler, J., Leach, S., Zhang, G. (**2020**) JMJD5 couples with CDK9 to release the paused RNA polymerase II. *Proc. Natl. Acad. Sci. U.S.A 117* (33), 19888. DOI: 10.1073/pnas.2005745117
19. Melo, F. R., Wallerman, O., Paivandy, A., Calounova, G., Gustafson, A.-M., Sabari, B. R., Zabucchi, G., Allis, C. D., Pejler, G. (**2017**) Tryptase-catalyzed core histone truncation: A novel epigenetic regulatory mechanism in mast cells. *J. Allergy Clin. Immunol. 140* (2), 474-485. DOI: 10.1016/j.jaci.2016.11.044
20. Shen, J., Xiang, X., Chen, L., Wang, H., Wu, L., Sun, Y., Ma, L., Gu, X., Liu, H., Wang, L., Yu, Y.-n., Shao, J., Huang, C., Chin, Y. E. (**2017**) JMJD5 cleaves monomethylated histone H3 N-tail under DNA damaging stress. *EMBO rep. 18* (12), 2131-2143. DOI: 10.15252/embr.201743892
21. Schermerhorn, K. M. and Delaney, S. (**2014**) A chemical and kinetic perspective on base excision repair of DNA. *Acc. Chem. Res. 47* (4), 1238-1246. DOI: 10.1021/ar400275a
22. Levine, R. L., Yang, I.-Y., Hossain, M., Pandya, G. A., Grollman, A. P., Moriya, M. (**2000**) Mutagenesis induced by a single 1,N-6-ethenodeoxyadenosine adduct in human hells. *Cancer Res. 60* (15), 4098-4104.

23. Riazuddin, S. and Lindahl, T. (**1978**) Properties of 3-methyladenine-DNA glycosylase from Escherichia coli. *Biochemistry 17* (11), 2110-2118. DOI: 10.1021/bi00604a014
24. El Ghissassi, F., Barbin, A., Nair, J., Bartsch, H. (**1995**) Formation of 1,N6-ethenoadenine and 3,N4-ethenocytosine by lipid peroxidation products and nucleic acid bases. *Chem. Res. Toxicol. 8* (2), 278-283. DOI: 10.1021/tx00044a013
25. Guengerich, F. P., Crawford, W. M., Watanabe, P. G. (**1979**) Activation of vinyl chloride to covalently bound metabolites: roles of 2-chloroethylene oxide and 2-chloroacetaldehyde. *Biochemistry 18* (23), 5177-5182. DOI: 10.1021/bi00590a023
26. Nair, U., Bartsch, H., Nair, J. (**2007**) Lipid peroxidation-induced DNA damage in cancer-prone inflammatory diseases: A review of published adduct types and levels in humans. *Free Radic. Biol. Med. 43* (8), 1109-1120. DOI: 10.1016/j.freeradbiomed.2007.07.012
27. O'Brien, P. J. and Ellenberger, T. (**2004**) Dissecting the broad substrate specificity of human 3-methyladenine-DNA glycosylase. *J. Biol. Chem. 279* (11), 9750-9757. DOI: 10.1074/jbc.M312232200
28. Kennedy, E. E., Li, C., Delaney, S. (**2019**) Global repair profile of human alkyladenine DNA glycosylase on nucleosomes reveals DNA packaging effects. *ACS Chem. Biol. 14* (8), 1687-1692. DOI: 10.1021/acschembio.9b00263
29. Li, C. and Delaney, S. (**2019**) Histone H2A variants enhance the initiation of base excision repair in nucleosomes. *ACS Chem. Biol. 14* (5), 1041-1050. DOI: 10.1021/acschembio.9b00229
30. Bilotti, K., Tarantino, M. E., Delaney, S. (**2018**) Human oxoguanine glycosylase 1 removes solution accessible 8-oxo-7,8-dihydroguanine lesions from globally substituted nucleosomes except in the dyad region. *Biochemistry 57* (9), 1436-1439. DOI: 10.1021/acs.biochem.7b01125
31. Luger, K., Rechsteiner, T. J., Richmond, T. J. (**1999**) Expression and purification of recombinant histones and nucleosome reconstitution. *Methods Mol. Biol. 119*, 1-16. DOI: 10.1385/1-59259-681-9:1
32. Luger, K., Rechsteiner, T. J., Richmond, T. J. (**1999**) Preparation of nucleosome core particle from recombinant histones. *Methods Enzymol. 304*, 3-19. DOI: 10.1016/S0076-6879(99)04003-3
33. Hayes, J. J., Tullius, T. D., Wolffe, A. P. (**1990**) The structure of DNA in a nucleosome. *Proc. Natl. Acad. Sci. U.S.A 87* (19), 7405-7409. DOI: 10.1073/pnas.87.19.7405.
34. Jain, S. S. and Tullius, T. D. (**2008**) Footprinting protein–DNA complexes using the hydroxyl radical. *Nat. Protoc. 3* (6), 1092-1100. DOI: 10.1038/nprot.2008.72
35. Das, R., Laederach, A., Pearlman, S. M., Herschlag, D., Altman, R. B. (**2005**) SAFA: semi-automated footprinting analysis software for high-throughput quantification of nucleic acid footprinting experiments. *RNA 11* (3), 344-54. DOI: 10.1261/rna.7214405
36. Vasudevan, D., Chua, E. Y. D., Davey, C. A. (**2010**) Crystal structures of nucleosome core particles containing the '601' strong positioning sequence. *J. Mol. Biol. 403* (1), 1-10. DOI: 10.1016/j.jmb.2010.08.039
37. Caffrey, P. J., Kher, R., Bian, K., Li, D., Delaney, S. (**2020**) Comparison of the base excision and direct reversal repair pathways for correcting 1,N6-ethenoadenine in strongly positioned nucleosome core particles. *Chem. Res. Toxicol. 33* (7), 1888-1896. DOI: 10.1021/acs.chemrestox.0c00089
38. Balasubramanian, B., Pogozelski, W. K., Tullius, T. D. (**1998**) DNA strand breaking by the hydroxyl radical is governed by the accessible surface areas of the hydrogen atoms of the DNA backbone. *Proc. Natl. Acad. Sci. U.S.A 95* (17), 9738. DOI: 10.1073/pnas.95.17.9738

39. Samson, L., Derfler, B., Boosalis, M., Call, K. (**1991**) Cloning and characterization of a 3-methyladenine DNA glycosylase cDNA from human cells whose gene maps to chromosome 16. *Proc. Natl. Acad. Sci. U.S.A 88* (20), 9127-9131. DOI: 10.1073/pnas.88.20.9127
40. Chakravarti, D., Ibeanu, G. C., Tano, K., Mitra, S. (**1991**) Cloning and expression in Escherichia coli of a human cDNA encoding the DNA repair protein N-methylpurine-DNA glycosylase. *J. Biol. Chem. 266* (24), 15710-15715.
41. Olmon, E. D. and Delaney, S. (**2017**) Differential ability of five DNA glycosylases to recognize and repair damage on nucleosomal DNA. *ACS Chem. Biol. 12* (3), 692-701. DOI: 10.1021/acschembio.6b00921
42. Tarantino, M. E., Dow, B. J., Drohat, A. C., Delaney, S. (**2018**) Nucleosomes and the three glycosylases: High, medium, and low levels of excision by the uracil DNA glycosylase superfamily. *DNA Repair 72*, 56-63. DOI: 10.1016/j.dnarep.2018.09.008
43. Beard, B. C., Wilson, S. H., Smerdon, M. J. (**2003**) Suppressed catalytic activity of base excision repair enzymes on rotationally positioned uracil in nucleosomes. *Proc. Natl. Acad. Sci. U.S.A 100* (13), 7465-70. DOI: 10.1073/pnas.1330328100
44. Cole, H. A., Tabor-Godwin, J. M., Hayes, J. J. (**2010**) Uracil DNA glycosylase activity on nucleosomal DNA depends on rotational orientation of targets. *J. Biol. Chem. 285* (4), 2876-85. DOI: 10.1074/jbc.M109.073544
45. Hinz, J. M., Rodriguez, Y., Smerdon, M. J. (**2010**) Rotational dynamics of DNA on the nucleosome surface markedly impact accessibility to a DNA repair enzyme. *Proc. Natl. Acad. Sci. U.S.A 107* (10), 4646-4651. DOI: 10.1073/pnas.0914443107
46. Prasad, A., Wallace, S. S., Pederson, D. S. (**2007**) Initiation of base excision repair of oxidative lesions in nucleosomes by the human, bifunctional DNA glycosylase NTH1. *Mol. Cell. Biol. 27* (24), 8442-8453. DOI: 10.1128/MCB.00791-07
47. Beard, B. C., Stevenson, J. J., Wilson, S. H., Smerdon, M. J. (**2005**) Base excision repair in nucleosomes lacking histone tails. *DNA Repair 4* (2), 203-209. DOI: 10.1016/j.dnarep.2004.09.011
48. Beard, B. C., Wilson, S. H., Smerdon, M. J. (**2003**) Suppressed catalytic activity of base excision repair enzymes on rotationally positioned uracil in nucleosomes. *Proc. Natl. Acad. Sci. U.S.A 100* (13), 7465-7470. DOI: 10.1073/pnas.1330328100
49. Rodriguez, Y., Duan, M., Wyrick, J. J., Smerdon, M. J. (**2018**) A cassette of basic amino acids in histone H2B regulates nucleosome dynamics and access to DNA damage. *J. Biol. Chem. 293* (19), 7376-7386. DOI: 10.1074/jbc.RA117.000358
50. Chafin, D. R., Vitolo, J. M., Henricksen, L. A., Bambara, R. A., Hayes, J. J. (**2000)** Human DNA ligase I efficiently seals nicks in nucleosomes. *EMBO J 19* (20), 5492-501. DOI: 10.1093/emboj/19.20.5492
51. Meas, R., Smerdon, M. J., Wyrick, J. J. (**2015**) The amino-terminal tails of histones H2A and H3 coordinate efficient base excision repair, DNA damage signaling and postreplication repair in Saccharomyces cerevisiae. *Nucleic Acids Res. 43* (10), 4990-5001. DOI: 10.1093/nar/gkv372
52. Pepenella, S., Murphy, K. J., Hayes, J. J. (**2014**) Intra- and inter-nucleosome interactions of the core histone tail domains in higher-order chromatin structure. *Chromosoma 123* (1-2), 3-13. DOI: 10.1007/s00412-013-0435-8
53. Fu, I., Cai, Y., Zhang, Y., Geacintov, N. E., Broyde, S. (**2016**) Entrapment of a histone tail by a DNA lesion in a nucleosome suggests the lesion impacts epigenetic marking: a molecular dynamics study. *Biochemistry 55* (2), 239-242. DOI: 10.1021/acs.biochem.5b01166

54. Kan, P. Y., Caterino, T. L., Hayes, J. J. (**2009**) The H4 tail domain participates in intra- and internucleosome interactions with protein and DNA during folding and oligomerization of nucleosome arrays. *Mol Cell Biol 29* (2), 538-46. DOI: 10.1128/MCB.01343-08
55. Cai, Y., Fu, I., Geacintov, N. E., Zhang, Y., Broyde, S. (2018) Synergistic effects of H3 and H4 nucleosome tails on structure and dynamics of a lesion-containing DNA: Binding of a displaced lesion partner base to the H3 tail for GG-NER recognition. *DNA Repair 65*, 73-78. DOI: 10.1016/j.dnarep.2018.02.009
56. Ngo, T. T. M., Zhang, Q., Zhou, R., Yodh, J. G., Ha, T. (**2015**) Asymmetric unwrapping of nucleosomes under tension directed by DNA local flexibility. *Cell 160* (6), 1135-1144. DOI: 10.1016/j.cell.2015.02.001
57. Odell, I. D., Newick, K., Heintz, N. H., Wallace, S. S., Pederson, D. S. (**2010**) Non-specific DNA binding interferes with the efficient excision of oxidative lesions from chromatin by the human DNA glycosylase, NEIL1. *DNA Repair 9* (2), 134-143. DOI: 10.1016/j.dnarep.2009.11.005
58. Maher, R. L., Prasad, A., Rizvanova, O., Wallace, S. S., Pederson, D. S. (**2013**) Contribution of DNA unwrapping from histone octamers to the repair of oxidatively damaged DNA in nucleosomes. *DNA Repair 12* (11), 964-971. DOI: 10.1016/j.dnarep.2013.08.010
59. Lee, J. and Lee, T.-H. (**2017**) Single-molecule investigations on histone H2A-H2B dynamics in the nucleosome. *Biochemistry 56* (7), 977-985. DOI: 10.1021/acs.biochem.6b01252
60. Fu, I., Cai, Y., Geacintov, N. E., Zhang, Y., Broyde, S. (**2017**) Nucleosome histone tail conformation and dynamics: impacts of lysine acetylation and a nearby minor groove benzo[a]pyrene-derived Lesion. *Biochemistry 56* (14), 1963-1973. DOI: 10.1021/acs.biochem.6b01208
61. Bertin, A., Durand, D., Renouard, M., Livolant, F., Mangenot, S. (**2017**) H2A and H2B tails are essential to properly reconstitute nucleosome core particles. *Eur. Biophys. J. 36* (8), 1083-1094. DOI: 10.1007/s00249-007-0212-9
62. Andresen, K., Jimenez-Useche, I., Howell, S. C., Yuan, C., Qiu, X. (**2013**) Solution scattering and FRET studies on nucleosomes reveal DNA unwrapping effects of H3 and H4 Tail removal. *PLOS ONE 8* (11), e78587. DOI: 10.1371/journal.pone.0078587
63. Bertin, A., Renouard, M., Pedersen, J. S., Livolant, F., Durand, D. (**2007**) H3 and H4 histone tails play a central role in the interactions of recombinant NCPs. *Biophys. J. 92* (7), 2633-2645. DOI: 10.1529/biophysj.106.093815
64. Mao, P., Brown, A. J., Malc, E. P., Mieczkowski, P. A., Smerdon, M. J., Roberts, S. A., Wyrick, J. J. (**2017**) Genome-wide maps of alkylation damage, repair, and mutagenesis in yeast reveal mechanisms of mutational heterogeneity. *Genome Res. 27* (10), 1674-1684. DOI: 10.1101/gr.225771.117
65. Pich, O., Muinos, F., Sabarinathan, R., Reyes-Salazar, I., Gonzalez-Perez, A., Lopez-Bigas, N. (**2018**) Somatic and germline mutation periodicity follow the orientation of the DNA minor groove around nucleosomes. *Cell 175* (4), 1074-1087.e18. DOI: 10.1016/j.cell.2018.10.004
66. van Attikum, H. and Gasser, S. M. (**2009**) Crosstalk between histone modifications during the DNA damage response. *Trends Cell Biol. 19* (5), 207-217. DOI: 10.1016/j.tcb.2009.03.001
67. Montaldo, N. P., Bordin, D. L., Brambilla, A., Rösinger, M., Fordyce Martin, S. L., Bjørås, K. Ø., Bradamante, S., Aas, P. A., Furrer, A., Olsen, L. C., Kunath, N., Otterlei, M., Sætrom, P., Bjørås, M., Samson, L. D., van Loon, B. (**2019**) Alkyladenine DNA glycosylase associates with transcription elongation to coordinate DNA repair with gene expression. *Nat. Commun. 10* (1), 5460. DOI: 10.1038/s41467-019-13394-w

Table of Contents Graphic